Difference-quotient turbulence model: The axisymmetric isothermal jet

Peter W. Egolf[1] and Daniel A. Weiss[2,*]
[1]*Swiss Federal Laboratories for Materials Testing and Research, CH-8600 Dübendorf, Switzerland*
[2]*Laboratoire PMMH, École Supérieure de Physique et de Chimie Industrielles de la Ville de Paris, F-75231 Paris Cedex 05, France*

(Received 15 September 1997; revised manuscript received 18 March 1998)

Taking the difference-quotient turbulence model into consideration, the mean velocities and the second-order fluctuation correlations, also called Reynolds stresses, of the axisymmetric isothermal jet in a quiescent surrounding are analytically calculated. Three propositions are stated and proved. They relate a normalized turbulence fluctuation intensity and two turbulent energies on the center line of the jet to its spreading angle. The experiments confirm all propositions and several other model results convincingly.
[S1063-651X(98)03707-6]

PACS number(s): 47.27.Eq, 47.27.Ak

I. INTRODUCTION

In daily life turbulent round jets are ubiquitous fluid dynamic elements. For example, a variety of different jets occur at the outlet of hair dryers, in whirlpools, above overheated pressure cookers, in the vicinity of exhaust pipes, in gas and oil burners, and at outlets of aircraft power units. However, this fluid dynamic phenomenon does not have only technical applications. For example, if a candle light is blown out by a round turbulent jet of breathing air, this human-produced jet causes a second nonisothermal vertical plumelike jet to disappear. The fully developed isothermal axisymmetric jet is a fundamental example of free turbulence, which at present can only be calculated by empirical laws and is also apparently impossible to understand using first physical principles [1].

Wakes of different geometries and plane co- and counterflows are similar basic elements with a mean shear. Round jets are correctly interpreted as axisymmetric co- or counterflows. In the past century numerous experimental studies of basic fluid dynamic examples were performed by engineers. On the other hand, physicists are more concerned with field-theoretical aspects of turbulence, e.g., elimination of infrared divergences and renormalization [2], study of structure functions [3], anomalous scaling [4], multifractal nature [5], turbulent cascades and intermittency [6], and universality [7]. According to L'vov and Procaccia, the marriage of the physics and mathematics of turbulence with the engineering knowledge is a challenge ahead, which will last far into the 21st century [8].

Early theoretical results of the axisymmetric jet were obtained by applying the mixing-length hypothesis, introduced by Prandtl in 1925 [9]. One year later Tollmien [10], on this basis, calculated solutions of the mean downstream velocity, which show a slightly too narrow maxima symmetric to the axis of the jet. Schlichting, assuming a constant eddy viscosity, obtained better coincidence in the inner part of the jet, but with larger deviations far away from the center line (see, e.g., Ref. [11]). In a monumental monograph Abramovich [12] summarized all the available empirical theories of free jets, jets in finite spaces, turbulent jets in compressible gases, jets in the presence of flame fronts, etc.

Measurements of the mean velocity of round jets were performed using Pitot tubes. These measurements are well summarized by Hinze [13] (see also [14]). Later on most of the experimentally determined turbulence quantities were associated with Corrsin and co-workers [15–17]. More recent measurements were performed by Wygnanski and Fiedler [14] and Rodi [18]. In 1988 Hussein [19] applied hot wire and laser Doppler anemometry and more recently experimental results were published by Panchapakesan and Lumley performed in a round jet of air and a helium jet [20].

To restrict this treatise, out of the great variety of jets listed in the Introduction, only axisymmetric, fully developed turbulent jets are considered. Isothermal flows of pure liquids or gases without additional particles, e.g., pollutants and water vapor, are described. Therefore, reactive flows are also excluded. The jet behavior calculated is created by forced convection and not, for example, by buoyancy effects.

This article consists of derivations based on physical laws, but also contains some assumptions. These do not contain empirical constants and they figure neatly into existing theories and describe experimental data very well. We have tried to give the reader the possibility to distinguish strict results from model considerations only. Always when an assumption is introduced, an A has been placed in front of the corresponding equation number, e.g., see (A1) below, etc. The P denotes a proposition, e.g., (P47).

II. MOTIVATION OF THE DIFFERENCE-QUOTIENT MODEL

Because of the obvious insufficiency of local gradient-type turbulence transport, e.g., see the work of Corrsin [21] and the more recent work of Bernard and Handler [22], Hinze, Sonnenberg, and Builtjes [23] (see also Hinze's book on turbulence [13]) proposed, considering the turbulent shear stress analogously to the description of the usual shear stress of viscoelastic fluids [24], by including a memory behavior depending on the time variable τ,

*Present address: Daimler-Benz AG, Research and Technology, P.O. Box 2260, 89013 Ulm, Germany.

$$\overline{u_2' u_1'} = -\varepsilon \int_0^\infty d\tau\, \tilde{M}(\tau) \left[\frac{\partial \overline{u_1}}{\partial x_2}(t-\tau) + \frac{\partial \overline{u_2}}{\partial x_1}(t-\tau) \right],$$

$$\varepsilon \propto \chi_2 \overline{u_1}. \quad \text{(A1)}$$

The turbulent shear stress $\overline{u_2' u_1'}$ is a correlation of the velocity fluctuation u_1' in the x_1 direction with u_2' in the x_2 direction (compare Sec. V).

An equation of this type can also describe the decay of isotropic turbulence. This approach was based on earlier intuitive ideas of Prandtl [25]. Today, in turbulence research, we have some conceptual understanding of approach (A1), even though a detailed mathematical derivation from basic equations is, to our knowledge, yet to be found. When deriving the Reynolds equations containing time-averaged values, second-order moments appear. Further equations can be established to solve the problem also containing these second-order moments. However, then again, one-order-higher correlations, now third-order moments, appear in the expanding system of equations. Continuing, in the end, one has to solve a set of infinite partial differential equations. It is known that, in certain cases when scaling applies, such a set can be replaced by one equation only, with just a dependence on the lowest-order moment, but showing a time delay and/or a nonlocality [26]. Such a transformation is equal to the technique of making a closure and that is exactly the procedure introduced by the application of a turbulence model. In a closure, higher-order moments are described as functions of moments, which are at least one order smaller. With assumption (A1) the simplest case is considered, where the second-order correlation is given by a functional dependence on the first-order moments only and these are identical to the mean velocities $\overline{u_1}$ and $\overline{u_2}$.

In Eq. (A1) the modified eddy viscosity ε is directly proportional to a length scale χ_2 and the time-averaged velocity $\overline{u_1}$, respectively $(\overline{u_1} - \overline{u_1}_{\min})$. $\tilde{M}(\tau)$ denotes a memory function characteristic for the turbulent flow considered. Its dimension is $[\tau]^{-1}$. This approach is also meaningful because the production of turbulence is mainly driven by the gradient of the time-averaged velocity field reaching from the present back to some time when a time correlation vanishes. It is known that memory effects in time are the analog to nonlocalities in space. Because at the moment we are considering only quasistationary cases, it is useful to study Eq. (A1) in three-dimensional Euclidean space by replacing time by the transverse coordinate of the shear flow and the memory function $\tilde{M}(\tau)$ by a nonlocality function $\tilde{N}(x_2')$,

$$\overline{u_2' u_1'} = -\sigma \chi_2 (\overline{u_1} - \overline{u_1}_{\min}) \int_{-\infty}^{-\infty} dx_2' \tilde{N}(x_2, x_2') \frac{\partial \overline{u_1}}{\partial x_2}(x_2 - x_2'). \quad \text{(A2)}$$

The function σ is related to the Reynolds number. In Eq. (A2) the assumption of a flow with a large velocity gradient transverse to the direction of the main flow is considered, so that this gradient is at least one order larger than the one in the downstream direction with reverse indices. Therefore, the smaller gradient has been neglected. Because the nonlocality can be considered as a non-normalized probability function for the turbulent momentum transfer of eddies with different correlation lengths and corresponding radii, respectively, we generalize Eq. (A2),

$$\overline{u_2' u_1'} = -\sigma \chi_2 (\overline{u_1} - \overline{u_1}_{\min}) \frac{\int_{-\infty}^{\infty} dx_2' N(x_2, x_2') \frac{\partial \overline{u_1}}{\partial x_2}(x_2 - x_2')}{\int_{-\infty}^{\infty} dx_2' N(x_2, x_2')}. \quad \text{(3)}$$

The normalized nonlocality function $\tilde{N}$ considered has now been replaced by a non-normalized counterpart N. It can be described by a linear combination of Heaviside distributions (two-sided step ''functions'') or a characteristic function, respectively, with the properties

$$N(x_2, x_2') = \begin{cases} 0, & x_2' < x_2 \\ 1, & x_2 \leqslant x_2' \leqslant x_2 + \lambda \\ 0, & x_2 + \lambda < x_2'. \end{cases} \quad \text{(A4)}$$

Our approach states that equal contributions of the time-averaged velocity gradient occur in a space interval of correlation length λ. Substituting in Eq. (A4) $x_2 + \lambda$ by $x_{2_{\max}}$ and combining Eqs. (3) and (A4), it follows that

$$\overline{u_2' u_1'} = -\sigma \chi_2 (\overline{u_1} - \overline{u_1}_{\min}) \frac{\int_{x_2}^{x_{2_{\max}}} dx_2' \frac{\partial \overline{u_1}}{\partial x_2'}(x_2')}{\int_{x_2}^{x_{2_{\max}}} dx_2'}. \quad \text{(5)}$$

It is known that in many turbulent flows the mean velocity in the main flow direction can be separated in the order of the two variables x_1 and x_2. Therefore, with this assumption, the right-hand side of Eq. (5) can be integrated. This leads to the difference-quotient turbulence model (DQTM), which was developed several years ago by completely other means (see Ref. [27]):

$$\overline{u_2' u_1'}(x_1, x_2) = -\sigma \chi_2 [\overline{u_1}(x_1, x_2) - \overline{u_1}_{\min}(x_1)] \times \frac{\overline{u_1}_{\max}(x_1) - \overline{u_1}(x_1, x_2)}{x_{2_{\max}} - x_2}. \quad \text{(6)}$$

χ_2 is a characteristic length of the flow problem, perpendicular to the main flow direction. The quantity $x_{2_{\max}}$ denotes the space coordinate, where $\overline{u_1}$ takes its maximum or supremum as a function of the variable x_2.

In 1994, by applying the difference-quotient turbulence model, it was shown that the available simple turbulence models only relate to one or at maximum two eddy sizes and therefore are not expected to produce more than approximate solutions. The DQTM, which is a generalization of Prandtl's mixing-length theory and corresponds to an infinite set of eddy sizes, produces several simple analytical results, e.g., axial and radial profiles of turbulence intensities, for wakes [27], the plane Couette flow [28], and the plane Poiseuille flow [29], all agreeing well with experimental data. The wake flow also defines a free turbulent flow problem and the Couette and Poiseuille flows are ''wall-turbulent'' shear

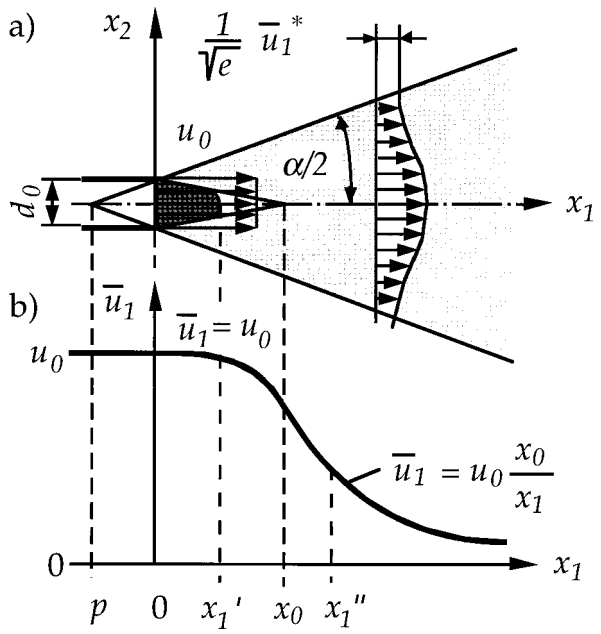

FIG. 1. A turbulent round jet is emerging from a nozzle with diameter d_0. According to current theory, the fictitious core length x_0 is used in the description of the problem (a). In a projection the time-averaged velocity component in the longitudinal direction on the center line is shown (b), which is constant in the core region ($x_1 < x_1'$). After a transition region ($x_1' < x_1 < x_1''$) in the self-similarity domain ($x_1'' < x_1$) the velocity is hyperbolic.

flows. In the two latter cases, in the differential equations and their solutions an order parameter occurs, being a function of the inverse Reynolds number. This naturally appearing order parameter was shown to be equivalent to the production of turbulent kinetic energy in the entire domain per unit length in the downstream direction.

The equations in this section also lead to ideas how the difference-quotient turbulence model could be generalized to describe more complex flows, e.g., with temporal behavior. However, this would be beyond the scope of this paper. Furthermore, they show how a simple scheme for numerical calculations, based on the DQTM, could be designed. In contrast to standard k-ε model applications, instead of one spatial derivative over large domains, arithmetic averages of directional derivatives would have to be taken into consideration.

III. BASIC EQUATIONS

When a fluid streams out of a round nozzle into an infinitely extended domain and the Reynolds number is very large

$$\mathrm{Re} = \frac{u_0 d_0}{\nu} \geqslant 25\,000, \tag{7}$$

then a fully developed turbulent jet is observed. Such a jet is drawn in Fig. 1. It has a linearly growing width in the downstream direction. The quantity d_0 denotes the diameter of the nozzle and u_0 the constant velocity of the laminar flow in the e_1 direction at the location $x_1 = 0$.

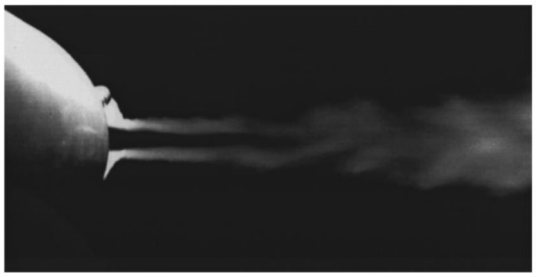

FIG. 2. Photograph of a jet. Smoke particles injected into the turbulent zones show an intense mixing and thus a visualization of the turbulent domains. Hardly any transport of smoke into the laminar core region takes place. Therefore, in a plane jet the core can clearly be detected photographically. Its parabolic time-averaged profile becomes transparent when the photographic exposure time is high.

The core region is parabolic (dark shaded domain) and has a length x_1', but in a simplified model it is drawn as triangle reaching to the fictitious core length x_0. A photograph of a plane jet, with analogous features, and its core is shown in Fig. 2. The domain $x_1 > x_1''$ is the self-similarity domain.

The fluid is assumed to be incompressible and the density ρ to be constant. All other physical quantities are separated into a time mean value and a corresponding fluctuation quantity, so that

$$\chi = \overline{\chi} + \chi', \quad \chi \in \{u_1, u_2, \ldots\} \tag{8a}$$

$$\overline{\chi'} = 0. \tag{8b}$$

Now operation (8a) is applied to the continuity and the Navier-Stokes equations. Taking the average of all the terms in these equations leads to the Reynolds equations. For a quasistationary state and for flows free from mean rotational motion

$$\overline{u}_3 = 0, \tag{9a}$$

$$\frac{\partial}{\partial x_3}\,\overline{\varphi} = 0, \quad \overline{\varphi} \in \{\overline{u}_1, \overline{u_1' u_3'}, \ldots\}, \tag{9b}$$

the following system is obtained [13]:

$$\frac{\partial \overline{u}_1}{\partial x_1} + \frac{1}{x_2}\frac{\partial}{\partial x_2}(x_2 \overline{u}_2) = 0, \tag{10}$$

$$\overline{u}_1 \frac{\partial \overline{u}_1}{\partial x_1} + \overline{u}_2 \frac{\partial \overline{u}_1}{\partial x_2} + \frac{1}{\rho}\frac{\partial \overline{p}}{\partial x_1} + \frac{\partial}{\partial x_1}\overline{u_1'^2} + \frac{1}{x_2}\frac{\partial}{\partial x_2}(x_2 \overline{u_2' u_1'}) = 0, \tag{11}$$

$$\overline{u}_1 \frac{\partial \overline{u}_2}{\partial x_1} + \overline{u}_2 \frac{\partial \overline{u}_2}{\partial x_2} + \frac{1}{\rho}\frac{\partial \overline{p}}{\partial x_2} + \frac{\partial}{\partial x_1}\overline{u_2' u_1'} + \frac{1}{x_2}\frac{\partial}{\partial x_2}(x_2 \overline{u_2'^2}) - \frac{1}{x_2}\overline{u_3'^2} = 0. \tag{12}$$

Because very large Reynolds numbers are assumed (7), the viscous terms in the momentum equations are neglected. Applying a scale analysis [13], one obtains a reduced equation compared to Eq. (12),

$$\frac{1}{\rho}\frac{\partial \overline{p}}{\partial x_2}+\frac{1}{x_2}\frac{\partial}{\partial x_2}(x_2\overline{u_2'^2})-\frac{1}{x_2}\overline{u_3'^2}=0. \tag{13}$$

At this stage the assumption of isotropy of the fluctuation intensities is introduced

$$\overline{u_1'^2}=\overline{u_2'^2} \tag{A14a}$$

$$=\overline{u_3'^2}. \tag{A14b}$$

Only with Eq. (A14b) Eq. (13) reduces and can be integrated

$$\overline{p}+\rho\overline{u_2'^2}=p_0, \tag{15}$$

where p_0 denotes the undisturbed constant pressure far from the turbulence domain. To drop the pressure term in Eq. (11), Eq. (15) can be substituted

$$\overline{u_1}\frac{\partial \overline{u_1}}{\partial x_1}+\overline{u_2}\frac{\partial \overline{u_1}}{\partial x_2}+\frac{\partial}{\partial x_1}(\overline{u_1'^2}-\overline{u_2'^2})+\frac{1}{x_2}\frac{\partial}{\partial x_2}(x_2\overline{u_2'u_1'})=0. \tag{16}$$

After applying assumption (A14a) to cancel the third term, it follows that

$$\overline{u_1}\frac{\partial \overline{u_1}}{\partial x_1}+\overline{u_2}\frac{\partial \overline{u_1}}{\partial x_2}+\frac{1}{x_2}\frac{\partial}{\partial x_2}(x_2\overline{u_2'u_1'})=0. \tag{17}$$

In this reduced form the momentum equation is applied. It is important to stress that the third and fourth terms in Eq. (11) cannot be neglected by magnitude of order estimates as they are both of the same order as the fifth term (e.g., compare maxima in Figs. 5 and 8).

IV. SELF-SIMILARITY

From experimental observations it is known that for all $x_1>x_1''$ a self-similarity domain exists (Fig. 1), where the mean physical quantities can be made dimensionless to become functions of only one variable. This leads to the possibility of transforming the two partial differential equations (10) and (17) into a single ordinary differential equation. The following self-similarity relations are assumed to hold. Distances from the pole x_1-p are replaced by x_1 because in the self-similarity domain $x_1 \gg |p|$:

$$\overline{u_1}=u_0\left(\frac{x_1}{x_0}\right)^{p_1}f_1(\eta), \tag{18}$$

$$\overline{u_2}=u_0\left(\frac{x_1}{x_0}\right)^{p_2}f_2(\eta), \tag{19}$$

$$\overline{u_2'u_1'}=-u_0^2\left(\frac{x_1}{x_0}\right)^{p_{2,1}}f_{21}(\eta), \tag{20}$$

$$\eta=\frac{x_2}{b}, \tag{21a}$$

$$b=\beta\left(\frac{x_1}{x_0}\right)^{p_0}x_0. \tag{21b}$$

Substituting these relations into the continuity equation (10) leads to

$$p_1 f_1-p_0\eta\frac{df_1}{d\eta}+\frac{1}{\beta}\frac{1}{\eta}\frac{d}{d\eta}(nf_2)=0, \tag{22}$$

where

$$p_0+p_1-p_2=1 \tag{23}$$

had to be assumed to obtain self-similarity. Similarly, the momentum equation yields three equations

$$p_1 f_1^2-p_0\eta f_1\frac{df_1}{d\eta}+\frac{1}{\beta}\left[f_2\frac{df_1}{d\eta}-\frac{1}{\eta}\frac{d}{d\eta}(\eta f_{21})\right]=0, \tag{24}$$

$$p_0+2p_1-p_{21}=1, \tag{25a}$$

$$p_0+p_1=0. \tag{25b}$$

The system containing the three equations (23), (25a) and (25b) with the variables p_0, p_1, p_2, and $p_{2,1}$ cannot yet be solved definitively. A further relation is needed for that purpose. It follows from the self-similarity of the Reynolds shear stress

$$\frac{\overline{u_2'u_1'}}{\overline{u_1^{*2}}}=-f_{21}(\eta), \tag{26a}$$

$$\overline{u_1^*}(x_1)=\overline{u_1}(x_1,0) \tag{26b}$$

and is

$$2p_1-p_{21}=0. \tag{27}$$

Finally, the solution of Eqs. (23), (25a), (25b), and (27) can easily be determined,

$$p_0=1, \tag{28a}$$

$$p_1=-1, \tag{28b}$$

$$p_2=-1, \tag{28c}$$

$$p_{21}=-2. \tag{28d}$$

After a substitution of Eqs. (28a) and (28b) into Eq. (22) one obtains the continuity equation

$$f_1+\eta\frac{df_1}{d\eta}-\frac{1}{\beta}\frac{1}{\eta}\frac{d}{d\eta}(\eta f_2)=0, \tag{29}$$

and analogously the momentum equation (24) alters to

$$f_1^2+\eta f_1\frac{df_1}{d\eta}-\frac{1}{\beta}\left[f_2\frac{df_1}{d\eta}-\frac{1}{\eta}\frac{d}{d\eta}(\eta f_{21})\right]=0. \tag{30}$$

At present only two equations exist for the three functions f_1, f_2, and $f_{2,1}$. Therefore, as pointed out in Sec. II, a closure or a turbulence model is demanded. Thus, at this stage the DQTM is applied.

V. MEAN VELOCITIES AND THE REYNOLDS SHEAR STRESS

The normalized mean velocity in the radial direction is derived by a partial integration of a rearranged equation (29)

$$f_2=\beta\left[\eta f_1-\frac{1}{\eta}\int_0^{\eta} f_1(\xi)\,\xi\,d\xi\right]. \tag{31}$$

Now the DQTM is introduced. From Fig. 1(a) one can immediately see that

$$x_{2_{\max}}=0, \tag{32a}$$

$$\overline{u}_{1_{\min}}=0, \tag{32b}$$

$$\overline{u}_{1_{\max}}=\overline{u}_1^{*}(x_1). \tag{32c}$$

The quantity b defines the width of the jet, where the kinetic energy of the mean motion in the x_1 direction $\frac{1}{2}\rho\overline{u}_1^2$ decays to the fraction $1/e$. Then we obtain

$$\sigma=\frac{db}{dx_1} \tag{33a}$$

$$=\beta, \tag{33b}$$

$$\beta=\tan\left(\frac{\alpha}{2}\right). \tag{33c}$$

It is clear that a higher Reynolds stress is related to a larger spreading angle α of the jet. From Eqs. (6) and (32) it follows that

$$f_{21}=-\beta\,\frac{1}{\eta}\,f_1(1-f_1). \tag{34}$$

Equations (31) and (34) are inserted into Eq. (30). These substitutions lead to

$$\int_0^{\eta} f_1(\xi)\,\xi\,d\xi=1-2\,f_1-\eta\,\frac{f_1^2}{f_1'}, \tag{35a}$$

$$f_1'=\frac{df_1}{d\eta}. \tag{35b}$$

Taking the derivative of Eq. (35a) yields a highly nonlinear ordinary differential equation for the mean flow velocity in the axial direction

$$\eta f_1^2 f_1''-2(f_1')^3-3\,\eta f_1(f_1')^2-f_1^2 f_1'=0. \tag{36}$$

The solution of the differential equation is

$$f_1=\exp(-\tfrac{1}{2}\eta^2). \tag{37}$$

In Fig. 3 the analytical solution for the axial mean velocity is compared with the experimental data from Ref. [14]. When the solution of f_1 is inserted into Eq. (31), the mean velocity in the radial direction is obtained

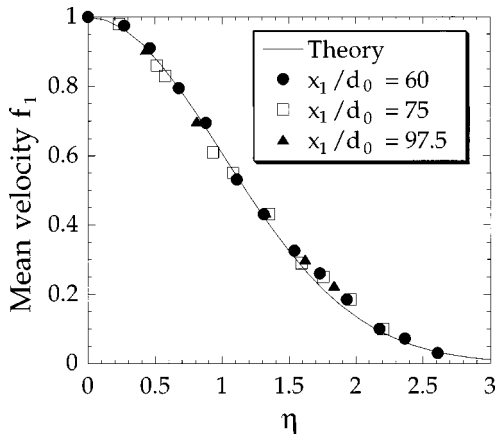

FIG. 3. Experimental data of the time-averaged velocity component in the downstream direction, taken from Ref. [14]. These are compared with theoretical results calculated by applying the DQTM. The measured points lie very close to the Gaussian distribution function (37).

$$f_2=\beta\left\{\eta\,\exp\left(-\frac{1}{2}\,\eta^2\right)-\frac{1}{\eta}\left[1-\exp\left(-\frac{1}{2}\,\eta^2\right)\right]\right\}. \tag{38}$$

From Eqs. (37) and (38) it follows immediately that

$$f_2=\beta\left[\eta f_1-\frac{1}{\eta}\,(1-f_1)\right]. \tag{39}$$

To compare model results with experiments, the data of Wygnanski and Fiedler [14] have been chosen. The reason for this is that they also have published information on the radial velocity profile (see Fig. 4). A further comparison has been added to the figure. The experimental results of Fig. 3 have been inserted into Eq. (39) to obtain mean velocities in the radial direction shown for three distances downstream, which are presented by open markers. In the domain $\eta=1.4,\ldots,2.4$ the experimental data are slightly higher than the corresponding quantities stemming from the calculated function. Otherwise the agreement is good.

From Eqs. (34) and (37) one obtains the radial shear stress distribution

$$f_{21}=-\beta\,\frac{1}{\eta}\left[\exp\left(-\frac{1}{2}\,\eta^2\right)-\exp(-\eta^2)\right]. \tag{40}$$

In Fig. 5, besides the agreement with theoretical results, the mapping together of the different extracted experimental data, those represented by a D and the others marked by an I, is a very reliable test of the performance of the difference-quotient turbulence model.

VI. ENTRAINMENT

The mass flow rates can be derived from the mean velocities. The mass flux in axial direction is

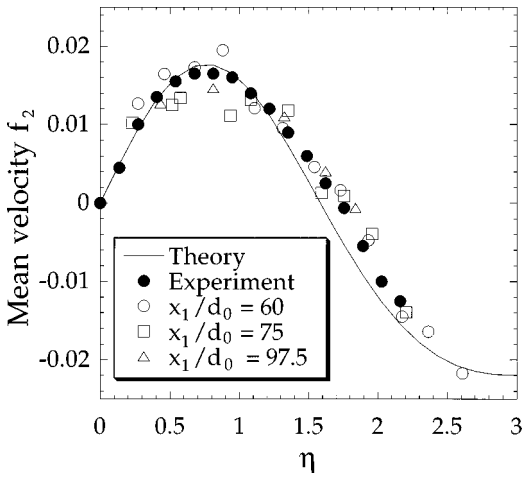

FIG. 4. Theoretical results are compared with the data from measurements given in Ref. [14]. The open markers denote transformed experimental data shown in Fig. 3. The radial mean velocity is less than 2% of the axial mean velocity. The condition $f_2<0$ describes domains where the flow vectors point toward the axis. Here entrainment of ambient air into the jet occurs.

$$m_1 = 2\pi\rho \int_0^\infty \overline{u_1} x_2 dx_2 . \tag{41}$$

The outgoing mass flow at the nozzle exit is

$$m_0 = \rho\pi \frac{d_0^2}{4} u_0 . \tag{42}$$

Inserting Eq. (37) into Eq. (41) and dividing by Eq. (42) leads to

$$\frac{m_1}{m_0} = k_1 \left(\frac{x_1}{d_0} \right) \tag{43a}$$

$$= 8 \frac{\beta^2}{m^2} \left(\frac{x_1}{x_0} \right), \tag{43b}$$

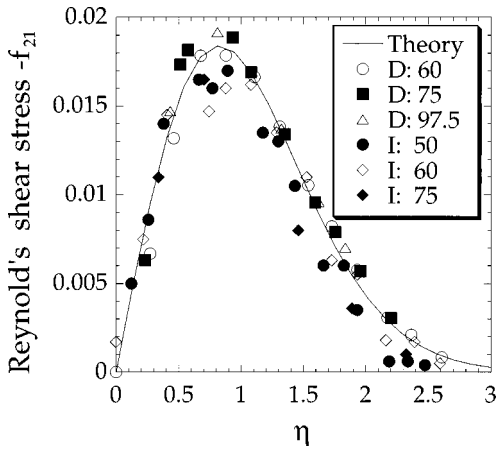

FIG. 5. The directly measured Reynolds shear stresses are denoted by a D. The number after the capital letter D denotes the distance downstream from the nozzle and is measured in units of d_0. The three Reynolds shear stresses, represented by an I, were calculated by taking the data of f_1 shown in Fig. 3 and then applying Eq. (34).

$$k_1 = 8 \frac{\beta^2}{m}, \tag{43c}$$

where the definition of the mixing number

$$m = \frac{d_0}{x_0} \tag{44}$$

has been introduced. It is the dimensionless ratio of the tube diameter d_0 and the fictitious core distance x_0. The mixing number shows values of

$$m = 0.15 - 0.18. \tag{45}$$

when jets emerge from round nozzles.

Ricou and Spalding [30] also report a linear behavior of the mass flux as a function of the axial distance x_1. After a reviewing process they conclude that the values of the constant k_1 obtained [see Eqs. (43a) and (43c)] range from about 0.22 up to 0.404 according to the investigators. Their own experimentally determined value of this constant is 0.32. They further comment that in the present state of turbulence theory the constant k_1 can only be determined by experimental means. In Sec. VII it is shown that with high accuracy we have

$$m = 2\beta \tag{46a}$$

$$\Leftrightarrow k_1 = 4\beta. \tag{46b}$$

Ricou and Spalding do not mention the spreading angle or the spreading parameter. However, from $k_1 = 0.32$, with Eq. (46b), β is now determined to be 0.080, which certainly must be close to its actual value (compare, e.g., in Ref. [14] $\beta = 0.074$ or in Ref. [20] $\beta = 0.082$). The experimental results of Ricou and Spalding are shown in Fig. 6. There is no doubt that the mass flow is very accurately a linear function of x_1.

VII. A PROPOSITION AND THE REYNOLDS NORMAL STRESSES

At the beginning of this section a proposition is introduced, which in the remainder of the section is proved in the context of the DQTM.

Proposition. The relative turbulence intensity in the downstream direction on the axis of the jet in the self-similarity domain is identical to the square root of its spreading parameter

$$\sqrt{\overline{u_1'^2}}/\overline{u_1^*} = \sqrt{\beta}. \tag{P47}$$

The definition of the normalizing quantity of the fluctuation intensity has been presented in Sec. V [see Eq. (32c)].

In this article, no reference is made to known relations between potential core lengths and spreading angles of jets (Fig. 1) (see, e.g., [31]). The aim of this section is to determine the normal turbulence stresses in the three space directions. From the DQTM, by replacing all second indices by the first $(2 \rightarrow 1)$, the following second-order correlation function is obtained:

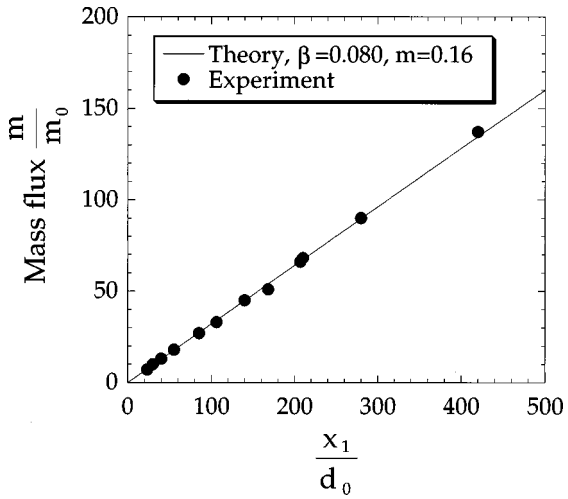

FIG. 6. The linear dependence of the mass flux in axial direction on the distance downstream from the origin of the jet also follows from dimensional analysis. The theory presented, based on the DQTM, yields different relations, which also match very well numerically. In this figure a comparison of theoretical and experimental data from Ref. [30] is shown.

$$\overline{u_1'^2} = -\sigma\chi_1(\overline{u}_1 - \overline{u}_{1_{\min}})\frac{\overline{u}_{1_{\max}} - \overline{u}_1}{x_{1_{\max}} - x_1}, \tag{A48a}$$

$$x_{1_{\max}} := \{x_1 | \overline{u}_1 = \max_{x_1}\{\overline{u}_1\}\}. \tag{A48b}$$

From Fig. 1 the following obvious relations are extracted:

$$\chi_1 = x_0, \tag{49a}$$

$$x_{1_{\max}} = x_0, \tag{49b}$$

$$\overline{u}_{1_{\min}} = 0, \tag{49c}$$

$$\overline{u}_{1_{\max}} = u_0, \tag{49d}$$

together with solutions already introduced in previous sections [see Eqs. (33a) and (33b)]. It is meaningful that the characteristic length in the longitudinal direction χ_1 is identical to the only available length in this direction, the core distance x_0. Inserting the values just determined into Eq. (48a) and slightly rearranging the following equations are obtained:

$$f_{11} = \frac{\overline{u_1'^2}}{\overline{u_1^{*2}}} \tag{50a}$$

$$= \left(\frac{\frac{x_1}{x_0} - f_1}{\frac{x_1}{x_0} - 1}\right)\beta f_1, \tag{50b}$$

$$\overline{u}_1^* = u_0\left(\frac{x_0}{x_1}\right), \tag{50c}$$

$$g_{11} = \sqrt{f_{11}}. \tag{50d}$$

With Eqs. (50a)–(50d) the normal stress was calculated [see Fig. 7(a)]. Corresponding measurements are shown in Fig. 7(b).

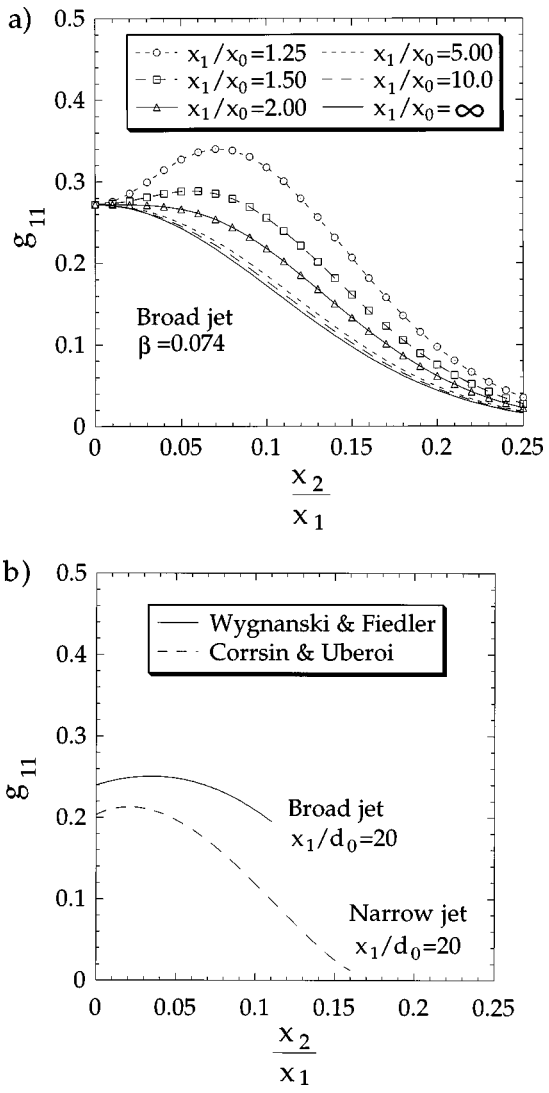

FIG. 7. Fluctuation intensities in the longitudinal direction for different distances downstream. The (b) experimentally observed off axis peaks at small distances (from Refs. [14,16]) are also observable in the (a) theoretical results. In accordance with the proposition, when an experimental jet shows a higher fluctuation intensity on the axis the spreading angle is also larger.

At large distances from the nozzle, because $0 \leqslant f_1 \leqslant 1$ according to Eq. (37), the self-preservation increases and the solution (50b) becomes completely self-similar,

$$f_{11} = \beta f_1(\eta), \quad x_1 \gg x_0. \tag{51}$$

Equation (50b) suggests the following limit to the relative fluctuation intensity on the axis of the jet:

$$g_{11} = \sqrt{\beta}\sqrt{\frac{f_1(0)\left[\frac{x_1}{x_0} - f_1(0)\right]}{\frac{x_1}{x_0} - 1}} \tag{52a}$$

$$= \sqrt{\beta} \tag{52b}$$

$$= \text{const}, \tag{52c}$$

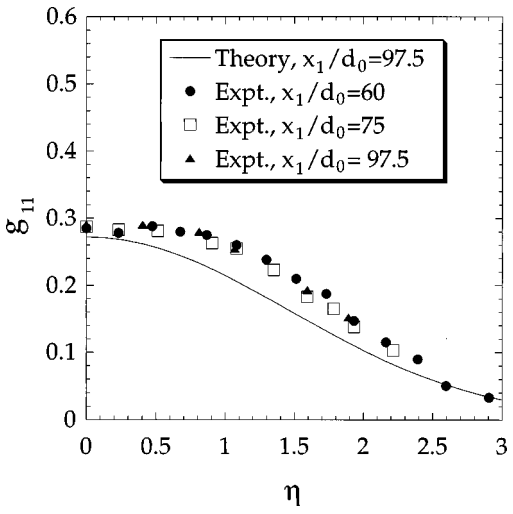

FIG. 8. The relative fluctuation intensity in the axial direction is shown. The experimental data stem from Ref. [14]. The deviation of the theoretical function from the experimental results at mean distances η is related to the production of turbulent kinetic energy and an incomplete turbulent transport of this kind of energy.

because $f_1(0)=1$. The final result (52b) ''proves'' the proposition on the basis of the DQTM. However, it must be remembered that the model has not yet been rigorously derived from first principles.

The jet measured by Corrsin and Uberoi [16] is narrower than the one that was experimentally investigated by Wygnanski and Fiedler [14] [Fig. 7(b)]. This completely corresponds to the presented theory, which states that the fluctuation intensity on the axis (see in the same figure at $x_2/x_1=0$) is smaller in the case of a narrower jet. However, this only qualitatively confirms proposition (P47) by measurements. More reliable comparisons of theoretical predictions and experimental data of the normal stress in the axial direction are shown in Fig. 8. The deviation of measurements from the theoretical results varies to a great extent on the experimental work taken into consideration in each case. For example, in Ref. [32] it was reported that in many experiments self-preservation was not attained completely. The lack of self-preservation leads to deviations. It is believed that these deviations, occurring at medium x_2/x_1 only, are caused by the underlying production of turbulent kinetic energy and that fluctuation energy has not been perfectly distributed over the whole width of the jet by transportation by the mean motion and turbulent convection. For example, better agreement has been obtained in experiments performed in a helium jet [20]. Wygnanski and Fiedler [14] interpret the deviations as follows: ''The fact that the longitudinal intensity contains more of its energy at the lower part of the spectrum is indicative of the manner in which the energy is being transferred, namely from the mean motion to u_1', and only then to u_2' and u_3'.''

Because the agreement is good at $x_2=0$, from measured data the following results are obtained, which provide a confirmation of proposition (P47) by experiments: The mean velocity profile (Fig. 3, β determined by curve fitting) $\beta=0.074$ and the axial fluctuation intensity (Fig. 8, $x_2/x_1=0$) $\sqrt{\beta}=0.28\Leftrightarrow\beta=0.079$. Following the statement of proposition (P47), from one set of experimental data, β has been derived in two different ways. The deviation of the two results is small. This confirms the proposition.

To calculate u_2' and u_3' it is assumed that the second and third diagonal component of the Reynolds tensor show the same spatial distribution but with a slightly smaller intensity

$$\overline{u_2'^2}=\overline{u_3'^2} \tag{A53a}$$

$$=\frac{\gamma}{\beta}\,\overline{u_1'^2},\quad \gamma\leqslant\beta, \tag{A53b}$$

$$\text{isotropy}\ \Leftrightarrow\gamma=\beta. \tag{A53c}$$

The momentum conservation equation [20] is

$$M(x_1)=2\pi\rho\int_0^\infty\left(\overline{u_1}^2+\overline{u_1'^2}-\frac{\overline{u_2'^2}+\overline{u_3'^2}}{2}\right)x_2\,dx_2 \tag{54a}$$

$$=M(0) \tag{54b}$$

$$=\frac{\pi d_0^2}{4}\,\rho u_0^2. \tag{54c}$$

Panchapakesan and Lumley [20] have found experimentally that this conservation is valid within $\pm5\%$ deviation from $M(0)$ for distances $30\leqslant x_1/d_0\leqslant150$. For the self-similarity domain, substituting Eqs. (18), (50b), and (53b) into Eq. (54a), after a division by $\overline{u_1}^{*2}$ it follows that

$$\int_0^\infty\left[f_1^2+(\beta-\gamma)\,\frac{\dfrac{x_1}{x_0}-f_1}{\dfrac{x_1}{x_0}-1}\,f_1\right]\eta\,d\eta=\frac{1}{8\beta^2}\left(\frac{d_0}{x_1}\right)^2\left(\frac{u_0}{\overline{u_1}^*}\right)^2. \tag{55}$$

After the introduction of the Gaussian distribution function (37) into Eq. (55), with $\xi=\eta^2$, the following equation is obtained:

$$(\gamma-\beta-1)\int_0^\infty e^{-\xi}d\xi+\frac{x_1}{x_0}\left[\int_0^\infty e^{-\xi}d\xi+(\beta-\gamma)\int_0^\infty e^{-\xi/2}d\xi\right]$$
$$=\frac{1}{4\beta^2}\left(\frac{d_0}{x_0}\right)^2\left(\frac{x_1}{x_0}-1\right). \tag{56}$$

Applying Eq. (44), after some reductions in size, a simple relation follows:

$$\gamma=\beta-\frac{\left(1-\dfrac{m^2}{4\beta^2}\right)\left(1-\dfrac{x_1}{x_0}\right)}{2\dfrac{x_1}{x_0}-1}, \tag{57a}$$

$$\text{isotropy}\Leftrightarrow\beta=\gamma \tag{57b}$$

$$\Leftrightarrow m=2\beta. \tag{57c}$$

Note that Eq. (57c) is identical to Eq. (46a), which was used without a derivation at the previous stage to calculate the entrainment rate. An incomplete self-preserving state is characterized by $m>2\beta$. In Figs. 9(a) and 9(b) m is 2% higher

than 2β. Comparing the results of Figs. 8 and 9, we note that the experiments do not indicate isotropy on the axis, which is in contrast to results observed by other investigators (see, e.g., Refs. [15,32]), who found isotropic behavior in some domain around the jet axis. Such conditions are to be expected since production of turbulence in the middle of the jet is weak and the turbulence present is mainly due to transport by mean and turbulent motion. Because of the lack of self-preservation, the additional energy still contained in the axial fluctuation correlations at intermediate η (Fig. 8) is missing in the intensities in the radial and azimuthal directions [Figs. 9(a) and 9(b)]. This is why these contributions, which have reasonable profiles compared to model calculations, show smaller amplitudes in comparison to the results in Fig. 8.

VIII. TURBULENCE ENERGY BALANCE

The turbulent energy equation for an axisymmetric flow can be derived straightforwardly from the momentum equation [13]

$$p+c+d+\mathscr{p}+\mathscr{d}=0. \tag{58}$$

The first energy term in this equation is the description of production of turbulent kinetic energy

$$p=\overline{u_2'u_1'}\,\frac{\partial\overline{u_1}}{\partial x_2}+\overline{u_1'^2}\,\frac{\partial\overline{u_1}}{\partial x_1}+\overline{u_2'^2}\,\frac{\partial\overline{u_2}}{\partial x_2}. \tag{59}$$

The second term c describes the turbulent convection

$$c=\frac{\partial}{\partial x_1}(\overline{u_1}\,\overline{\varepsilon})+\frac{1}{x_2}\frac{\partial}{\partial x_2}(x_2\overline{u_2}\,\overline{\varepsilon}), \tag{60a}$$

$$\overline{\varepsilon}=\overline{u_1}^{*2}e, \tag{60b}$$

where e describes the dimensionless turbulent kinetic energy [see below, Eqs. (76a)–(76c)] and

$$\varepsilon=\tfrac{1}{2}u_i'u_i', \quad i\in\{1,2,3\}. \tag{61}$$

In Eq. (61) Einstein's summation convention is applied. The diffusion d is given by

$$d=\frac{\partial}{\partial x_1}(\overline{u_1\varepsilon})+\frac{1}{x_2}\frac{\partial}{\partial x_2}(x_2\overline{u_2\varepsilon}). \tag{62}$$

The quantity $\mathscr{p}$ denotes the pressure diffusion

$$\mathscr{p}=\frac{1}{\rho}\left[\frac{\partial}{\partial x_1}(\overline{u_1p})+\frac{1}{x_2}\frac{\partial}{\partial x_2}(x_2\overline{u_2p})\right] \tag{63}$$

and $\mathscr{d}$ the dissipation term

$$\mathscr{d}=\nu\,\overline{\frac{\partial u_i'}{\partial x_j}\frac{\partial u_i'}{\partial x_j}}. \tag{64}$$

The first two terms, which denote production and convection, contain correlations that have already been derived in this article. Therefore, they will be examined further. The last three contributions in Eq. (58) show additional correlations, which we intend to refer to in a subsequent work. Now a second proposition can be stated.

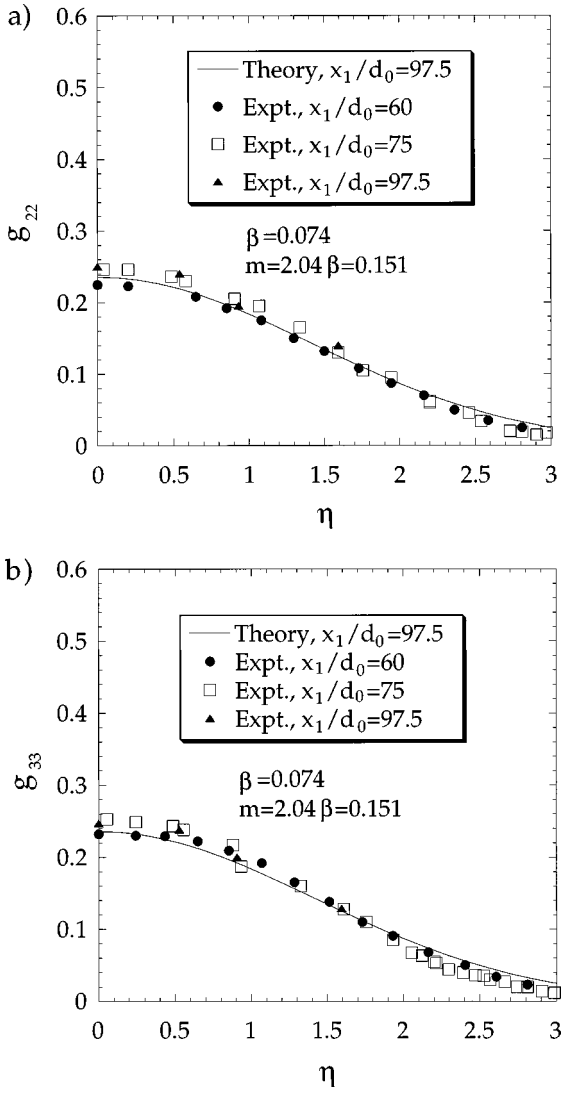

FIG. 9. Relative intensities in the (a) radial direction and (b) azimuthal direction. Experimental data have been copied from Ref. [14]. The functions g_{22} and g_{33} are defined as shown in Eqs. (50a)–(50d), but by taking the intensities in the x_2 and x_3 directions, respectively into consideration.

Proposition. The relative turbulent production $\pi(\eta)$ on the axis of the jet in the self-similarity domain is identical to minus half of the spreading parameter

$$\pi(0)=-\beta/2. \tag{P65}$$

The production p is made dimensionless

$$\pi=\frac{px_1}{\overline{u_1}^{*3}}. \tag{66}$$

It is straightforward to derive

$$\pi=x_1\left\{-f_{21}\frac{df_1}{d\eta}\frac{\partial\eta}{\partial x_2}+f_{11}\frac{1}{\overline{u_1}^{*}}\left[\frac{\partial\overline{u_1}^{*}}{\partial x_1}f_1+\overline{u_1}^{*}\frac{df_1}{d\eta}\frac{\partial\eta}{\partial x_1}\right]+f_{22}\frac{df_2}{d\eta}\frac{\partial\eta}{\partial x_2}\right\}. \tag{67}$$

With

$$\frac{\partial \eta}{\partial x_1} = -\eta \frac{1}{x_1}, \tag{68a}$$

$$\frac{\partial \eta}{\partial x_2} = \frac{1}{\beta x_1}, \tag{68b}$$

$$\frac{d\overline{u_1^*}}{dx_1} = -\frac{1}{x_1}\overline{u_1^*}, \tag{68c}$$

it follows that

$$\pi = -\frac{1}{\beta} f_{21} \frac{df_1}{d\eta} - f_{11}\left(f_1 + \eta \frac{df_1}{d\eta}\right) + \frac{1}{\beta} f_{22} \frac{df_2}{d\eta}. \tag{69}$$

Equation (34) is now inserted for f_{21}. Equation (39) yields the expression for f_2 and Eq. (51), with the isotropy assumption (A53c), leads to the function describing f_{11} and f_{22}. After several terms have canceled out, we obtain

$$\pi = \left(\frac{1}{\eta} f_1 \frac{df_1}{d\eta} + \beta \frac{1}{\eta^2} f_1\right)(1 - f_1) + \beta \frac{1}{\eta} f_1 \frac{df_1}{d\eta}. \tag{70}$$

From Eq. (37) it follows immediately that

$$\frac{df_1}{d\eta} = -\eta f_1. \tag{71}$$

With this equation, several simplifications can be applied. Then we obtain

$$\pi = f_1^3 - f_1^2\left(1 + \beta + \beta \frac{1}{\eta^2}\right) + \beta \frac{1}{\eta^2} f_1. \tag{72}$$

This equation is graphically shown in Fig. 10, where its results are compared with data obtained by measurements, again from Ref. [14]. The absolute value of the production term shows a maximum at finite η.

Applying a Taylor expansion to the exponential functions describing f_1 in Eq. (72) produces

$$\pi = \left(1 - \frac{3}{2}\eta^2\right) - (1 - \eta^2)\left(1 + \beta + \beta \frac{1}{\eta^2}\right) + \beta \frac{1}{\eta^2}\left(1 - \frac{1}{2}\eta^2\right) \tag{73a}$$

$$= \eta^2\left(\beta - \frac{1}{2}\right) - \frac{1}{2}\beta. \tag{73b}$$

Now the function on the axis, where $\eta = 0$, can be evaluated,

$$\pi(0) = -\tfrac{1}{2}\beta. \tag{74}$$

This is exactly the statement of the second proposition (P65). With $\beta = 0.074$ one obtains $\pi = -0.037$ (see in Fig. 10 at the location $\eta = 0$).

The third proposition is related to the convection term.

Proposition. The relative turbulent convection $\chi(\eta)$ on the axis of the jet in the self-similarity domain is identical to minus three times the spreading parameter

$$\chi(0) = -3\beta. \tag{P75}$$

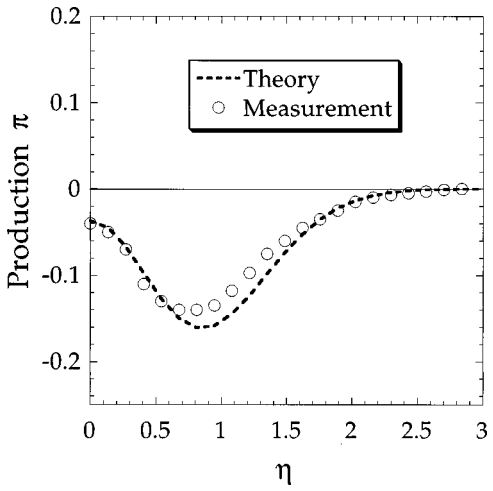

FIG. 10. The dimensionless turbulent production term extracted from measurements (from Ref. [14]) and calculated with the DQTM. The turbulent production term has a local maximum on the axis. Its numerical number is directly related to the spreading parameter.

The dimensionless turbulent kinetic energy e of the jet can be determined from some results derived in Sec. VII,

$$e(x_1, x_2) = \frac{1}{2} \frac{\overline{u_1'^2} + \overline{u_2'^2} + \overline{u_3'^2}}{\overline{u_1^*}^2} \tag{76a}$$

$$= \frac{\beta + 2\gamma}{2} \left(\frac{\frac{x_1}{x_0} - f_1}{\frac{x_1}{x_0} - 1}\right) f_1 \tag{76b}$$

$$\cong \frac{3}{2}\beta \left(\frac{\frac{x_1}{x_0} - f_1}{\frac{x_1}{x_0} - 1}\right) f_1. \tag{76c}$$

Again for simplicity only large distances $x_1 \gg x_0$ and isotropy of the fluctuations [see Eq. (76c)] are considered. Then

$$e = \frac{3}{2}\beta f_1. \tag{77}$$

Equation (60a) is then further developed

$$c = \frac{df_1}{d\eta}\frac{\partial \eta}{\partial x_1}\overline{u_1^*}^3 e + 3 f_1 \overline{u_1^*}^2 \frac{d\overline{u_1^*}}{dx_1} e + f_1 \overline{u_1^*}^3 \frac{de}{d\eta}\frac{\partial \eta}{\partial x_1} + \frac{1}{x_2} f_2 \overline{u_1^*}^3 e + \frac{df_2}{d\eta}\frac{\partial \eta}{\partial x_2}\overline{u_1^*}^3 e + f_2 \overline{u_1^*}^3 \frac{de}{d\eta}\frac{\partial \eta}{\partial x_2}. \tag{78}$$

With Eqs. (68a)–(68c) one obtains for the dimensionless convection term

$$\chi = \frac{c x_1}{\overline{u_1^*}^3} \tag{79}$$

the result

$$\chi = -\eta \frac{df_1}{d\eta} e - 3f_1 e - \eta f_1 \frac{de}{d\eta} + \frac{1}{\beta}\frac{1}{\eta} f_2 e + \frac{1}{\beta}\frac{df_2}{d\eta} e + \frac{1}{\beta} f_2 \frac{de}{d\eta}. \quad (80)$$

Inserting Eq. (39) together with Eq. (77) and after canceling a great number of terms a next intermediate result is

$$\chi = \frac{3}{2}\beta\left(2\frac{1}{\eta} f_1 \frac{df_1}{d\eta} - f_1^2 - \frac{1}{\eta}\frac{df_1}{d\eta}\right). \quad (81)$$

Substituting the solution (71), the final turbulent convection term reduces to an even more simple analytical expression than the production term (72),

$$\chi = \tfrac{3}{2}\beta f_1(1-3f_1). \quad (82)$$

This result is in very good coincidence with measurements derived by experimental means by Wygnanski and Fiedler [14]. Their curve, fitted to the measured data, is referred to in several articles and textbooks published in the years subsequent to their work.

Because $f_1(0)=1$, the special algebraic expression on the axis is

$$\chi(0) = \tfrac{3}{2}\beta f_1(0)[1-3f_1(0)] \quad (83a)$$

$$= -3\beta, \quad (83b)$$

which proves the third proposition (P75) on the basis of the DQTM and notably, without the occurrence of a single empirical constant. If $\beta=0.074$, then $\chi(0)=-0.222$ (compare with the numerical ordinate value in Fig. 11).

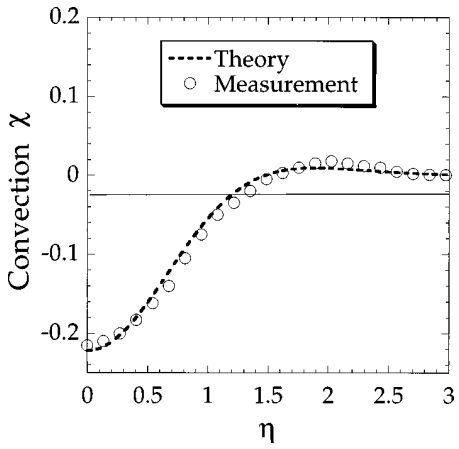

FIG. 11. The dimensionless turbulent convection term extracted from measurements (from Ref. [14]) and calculated with the DQTM. At $\eta=1.2$ the sign of this turbulence energy alters. The function takes a maximum at approximately $\eta=2.1$ and decreases toward infinity to zero.

IX. CONCLUSIONS

A nonlocal ansatz, which Prandtl and Hinze assumed to be a good basis for the development of a useful turbulence model, is taken to derive the DQTM. This derivation is not yet rigorous, but its features are at least compatible with generally accepted methods of turbulence modeling. Then a comprehensive theory of the axisymmetric isothermal jet, based on the DQTM, describing up to second order moments, is presented. Compared to existing similar models known to the authors, this presentation has the least number of empirical constants. In this theory it is shown that fluctuation quantities and turbulent energy terms on the jet axis are proportional to the spreading parameter of the jet. The mass flow at any cross section in the self-similarity domain downstream of the nozzle is also directly related to the spreading parameter. All the results are very simple analytical formulas. Their agreement with experimental data is good.

ACKNOWLEDGMENTS

We are very thankful to S. Altner, G. Gottschalk, and B. Poysden.

[1] B. Cipra, Science **272**, 951 (1996).
[2] V. L'vov and I. Procaccia, Phys. Rev. E **52**, 3840 (1995); **52**, 3858 (1995).
[3] F. Anselmet, Y. Gagne, J. Hopfinger, and R. A. Antonia, J. Fluid Mech. **140**, 63 (1984).
[4] V. Yakhot, Phys. Rev. E **49**, 2887 (1994).
[5] R. Benzi, G. Paladin, G. Parisi, and A. Vulpiani, J. Phys. A **17**, 3521 (1984).
[6] U. Frisch, *Turbulence—The Legacy of A. N. Kolmogorov*, 1st ed. (Cambridge University Press, Cambridge, 1995), Chaps. 6–8.
[7] S. Grossmann and D. Lohse, Phys. Rev. E **50**, 2784 (1994).
[8] V. L'vov and I. Procaccia, Phys. World **9**, 35 (1996).
[9] L. Prandtl, Z. Angew. Math. Mech. **5**, 136 (1925).
[10] W. Tollmien, Z. Angew. Math. Mech. **6**, 1 (1926).
[11] H. Schlichting, *Boundary Layer Theory* (McGraw-Hill, New York, 1961).
[12] G. N. Abramovich, *The Theory of Turbulent Jets* (MIT Press, Cambridge, MA, 1963).
[13] J. O. Hinze, *Turbulence* (McGraw-Hill, New York, 1975).
[14] I. Wygnanski and H. Fiedler, J. Fluid Mech. **38**, 577 (1969).
[15] S. Corrsin, NACA Wartime Report No. 94, 1943 (unpublished).
[16] S. Corrsin and M. S. Uberoi, NACA Report No. 1865, 1949.
[17] S. Corrsin and A. L. Kistler, NACA Report No. 1244, 1955.
[18] W. Rodi, DISA Information **17**, 9 (1975).
[19] H. J. Hussein, dissertation, State University of New York at Buffalo, 1988 (unpublished).
[20] N. R. Panchapakesan and J. L. Lumley, J. Fluid Mech. **246**, 197 (1993); **246**, 225 (1993).
[21] S. Corrsin, Adv. Geophys. **18A**, 25 (1974).
[22] P. S. Bernard and R. A. Handler, J. Fluid Mech. **220**, 99 (1990).
[23] J. O. Hinze, R. E. Sonnenberg, and P. J. H. Builtjes, Appl. Sci. Res. **29**, 1 (1974).

[24] R. S. Rivlin, Q. Appl. Math. **15**, 212 (1957).
[25] L. Prandtl, Z. Angew. Math. Mech. **18**, 77 (1938).
[26] Hao Bai-Lin, *Chaos* (World Scientific, Singapore, 1984).
[27] P. W. Egolf, Phys. Rev. E **49**, 1260 (1994).
[28] P. W. Egolf and D. A. Weiss, Phys. Rev. Lett. **75**, 2956 (1995).
[29] P. W. Egolf and D. A. Weiss, Helv. Phys. Acta **68**, 219 (1995).
[30] F. P. Ricou and D. B. Spalding, J. Fluid Mech. **38**, 577 (1969).
[31] P. W. Egolf, Gesund. Ing. **113**, 198 (1992).
[32] A. A. Townsend, *The Structure of Turbulent Shear Flow* (Cambridge University Press, Cambridge, 1956).